1661-8726/07/010071-14
DOI 10.1007/s00015-007-1206-4
Birkhäuser Verlag, Basel, 2007

Swiss j. geosci. 100 (2007) 71–84

C and O isotope stratigraphy in shallow-marine carbonate: a tool for sequence stratigraphy (example from the Lodève region, peritethian domain)

YOURI HAMON[1, 2] & GILLES MERZERAUD[1]

Key words: C and O isotope, shallow-marine carbonate, diagenesis, Lias, sequence stratigraphy.

ABSTRACT

Carbon and Oxygen isotope profiles from a well-dated carbonate section spanning the Sinemurian time on the Caussenard High (southeast France) are compared to sedimentological data and the results from sequence stratigraphy analysis, in order to discuss the origin of isotopic variations in a shallow-marine carbonate succession. The sedimentological study has enabled the identification of four types of depositional environments (peritidal, lagoonal, sand shoal, outer-shelf) that formed meter-scale cycles. The latter are arranged in two third-order cycles whose boundaries correspond to distinct $\delta^{13}C$ and $\delta^{18}O$ negative peaks (at the end of the Hettangian time and during Middle Sinemurian). The origin of the isotopic signals is discussed and several hypothesis are envisaged: sea water ageing, early meteoric diagenesis. Isotopic curves observed here seems to be related to early meteoric diagenesis linked to variations of third-order sea-level cycles rather than environmental factors (temperature, salinity).

RESUME

Sur la coupe du Perthus, située sur le Seuil Caussenard (Sud-Est de la France), quarante échantillons couvrant l'intervalle Sinémurien ont été prélevés pour des analyses d'isotopes stables (C et O) et comparer aux données sédimentologiques dans le but de discuter l'origine du signal isotopique dans une série carbonatée d'environnement peu profond. L'étude sédimentologique a permis l'identification de quatre grands types de faciès sédimentaires (péritidal, lagunaire, dunes sous-marines, plate-forme externe) qui forment des cycles d'échelles métriques. Ces derniers s'arrangent verticalement en deux cycles de troisième ordre dont les limites correspondent aux tendances négatives en $\delta^{13}C$ et $\delta^{18}O$ (deux tendances négatives ont été observées, la première à la fin de l'Hettangien, la seconde au Sinémurien Moyen). L'origine des variations du signal isotopique est discutée et plusieurs hypothèses sont examinées: «vieillissement» des masses d'eau, diagenèse précoce. Dans le cas étudié, les variations observées semblent être contrôlées par les phénomènes de diagenèse précoce liés aux variations eustatiques moyen terme (troisième ordre), plutôt que par les paramètres environnementaux (température, salinité).

Introduction

Over the past thirty years, an important number of publications (Craig 1965; Tucker & Wright 1992; Zeebe 2001, among others) has documented the use of isotopes as a tool for paleotemperature reconstitutions (oxygen) or identification of diagenetic fluids forming cements (carbonate and oxygen). These data are generally interpreted with cross-plot diagrams, allowing to detect diagenetic signals. Such chemostratigraphic studies were firstly developed in basin settings where diagenesis is supposedly less widespread (Renard 1984; Corbin et al. 2000; Rey & Delgado 2002) and then in shallow-platform settings (Ingram et al. 1996; Valladares et al. 1996; Buonocunto et al. 2002; Immenhauser et al. 2003). In these specific environments, lateral and temporal isotopic variations are more complex and discussed because of facies diversity or diagenesis, particularly for oxygen ($\delta^{18}O$).

This paper shows that $\delta^{13}C$ and $\delta^{18}O$ signals in shallow-water carbonate can be related to the relative sea-level variations, rather than environmental factors (temperature, salinity) and that isotopic signals in shallow-water carbonates have the potential for providing an excellent complementary tool to sequence stratigraphy. Two distinct approaches have therefore been used in order to investigate the relation between sequence and isotope stratigraphy: firstly, a sedimentological and sequential analysis; secondly a chemostratigraphic study.

Geological and palaeogeographic setting

Isotope chemostratigraphic data are reported here from the "Perthus" section, a continuously exposed Permian to Dogger section of the Lodève region (South-East France). This region, also called Caussenard High ("Seuil Caussenard"), separates

[1] Laboratoire Dynamique de la lithosphère (équipe Bassins), UMR 5573, case 060, Université Montpellier 2, Place E. Bataillon, 34095 Montpellier cedex 05.
[2] I.F.P. - Dpt. Stratigraphie / Sedimentologie (R1330R), 1 & 4 Avenue du Bois-Préau, 92852 Rueil-Malmaison Cedex, France.
E-mail: youri.hamon@ifp.fr; Gilles.Merzeraud@gm.univ-montp2.fr

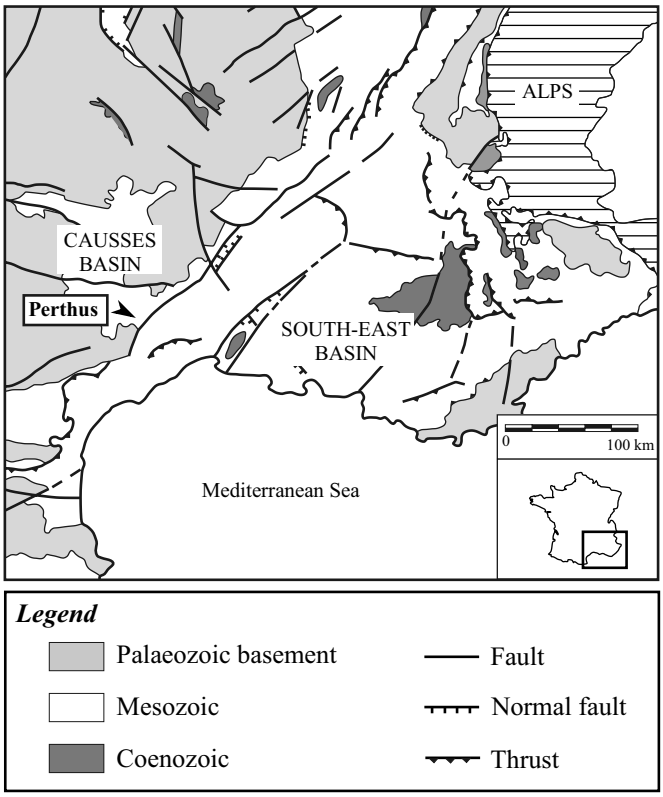

Fig. 1. Regional structural features in South-eastern France and location of the Perthus section.

the Causses Basin from the South-East Basin (Fig. 1). During the Early Jurassic, the Causses Basin was a large epeiric carbonate platform (50 x 100 km) located on the southwestern passive margin of the South-East Basin, corresponding to the westernmost part of the Tethysian ocean (Baudrimont & Dubois 1977; Debrand-Passard et al. 1984). From Hettangian to Toarcian time, this zone was affected by extensional tectonic movements, in relation to the first episode of opening of the Tethyan Ligurian Ocean. This extensional period was clearly recorded by the development of syn-sedimentary, SW-NE trending, normal faults (Cevennes fault, Nîmes fault) and rotation of fault blocks within the Liassic sediments (Baudrimont & Dubois 1977).

Liassic series of the Caussenard High (Fig. 2) can be subdivided into five lithological units (Marza et al. 1998): the two first units are Hettangian in age, whereas the third and fourth units (studied here) are Sinemurian in age. The last one is separated from the fourth unit by a major hardground and dated to be of Late Toarcian age. The first unit (30m thick) shows a calcareous facies succession from offshore bar grainstones, to inner shelf wackestones and to a final continental exposure (Lopez 1992). The second unit (200m thick) records a vertical stacking of meter-scale, shallowing-up, dolomitic peritidal cycles with emersive boundaries (Marza et al. 1998). The third and fourth units (ranging from 30 to 70 m in thickness) correspond to the studied series of this article and will be further developed. The fourth unit ended by a hardground of regional extension, that records condensation, erosion and dissolution features, and represents a hiatus of about 9 Ma (Lefavrais-Raymond & Lablanche 1985), from *Oxynotum* to *Spinatum* ammonite sub-zones. Then, a major change in sedimentation occurred, with the accumulation of black shales typical of deep-marine conditions.

All biostratigraphic units (ammonite biozone) for the Sinemurian series have been recognized (Fig. 2): Unit 3 covers the *Bucklandi*, *Semicostatum* and the lower part of the *Turneri* biozones, whereas unit 4 covers the upper part of the *Turneri*, *Obtusum* and the lower part of the *Oxynotum* biozones. The upper part of the *Oxynotum* biozone and the *Raricostatum* biozone are recorded in the top major hardground (Michard & Coumoul 1978; Perrisol 1990; Marza et al. 1998).

Facies analysis

The sinemurian series (units 3 and 4) were deposited on a shallow-water carbonate platform (Mélas 1982; Hamon 2004). Facies are organized in four genetically related facies assemblages. In order of increasing relative water depth, they comprise peritidal, lagoonal, sand shoal and outer-shelf facies.

Peritidal facies association

This facies assemblage mainly consists of dolomitic rocks. Bioturbated dolomicrite is composed of a homogeneous dolomicrite (Fig. 3A), showing a mottled appearance, with anastomosed burrow networks. Cryptalgal laminites (Fig. 3B) are composed of planar or smooth (locally crinkly), millimetre-sized laminae of dolomicrite, separated by thin (<1mm) and finely silty calcarenite laminae. Fenestral dolomicrite forms decimetre-scale units of micrite in which small millimetre-sized bird's eyes structures are randomly distributed. Subaerial exposure level constitute the final term of a gradual evolution involving the three preceding facies. Desiccation cracks are common and form polygonally arranged V-shaped mudcracks (Fig. 3C). Pedogenic horizons are generally 5–20 cm thick, grey to yellowish green in colour, and illite dominated (Mélas 1982). Decimetre-scale calcareous nodules occur within the claystone (Fig. 3D). Finally, karstification is represented by small irregular decimetric depressions, filled with decimetre-scale clasts and pebbles.

On the basis of many modern examples, the first three facies are interpreted to have formed in a shallow subtidal to upper intertidal environment. This is indicated by the absence of desiccation features, by the extremely sparse fauna (Wilson 1975). Finally, the presence of desiccation cracks, flat pebble conglomerate, pedogenic alteration or karstification phenomena is indicative of upper intertidal to supratidal environments (Pratt et al. 1992).

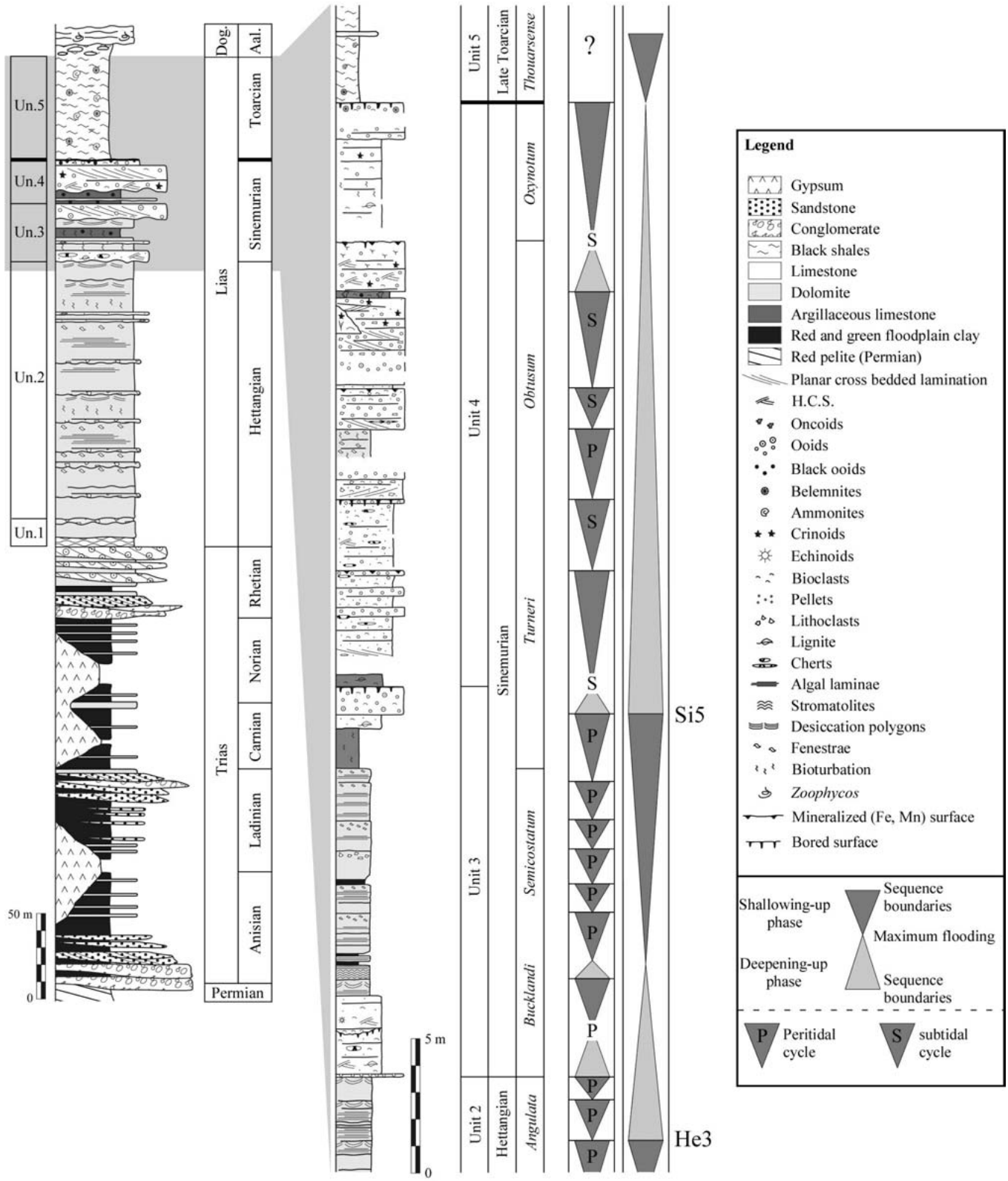

Fig. 2. Generalized Trias/Lias stratigraphy of the Lodève region, showing the stratigraphic position of the interval studied (shaded). A detailed section is presented with biostratigraphic units (ammonite biozone) and sequential interpretation (see text for explanation). Key for the sedimentologic logs and the sequential interpretation applied for this and the subsequent sections.

Lagoonal facies association

This assemblage includes: (i) oncoids wackestone; (ii) Bioturbated argillaceous mudstone. Oncoids wackestone forms decimetre-scale units, grey to light blue in colour. Oncoids have irregular shapes, are 0.5 to 2 cm in diameter, with nuclei of bioclasts, and microbial, organic-rich coatings. They are commonly associated with micritized ooids and bioclasts. Bioturbated argillaceous mudstone is composed of a bioturbated micrite, grey to blue in colour, organized in units ranging from 0.5 to 2 m in thickness. Numerous plant remains (dispersed leaves, twigs, wood fragments), coated with clay minerals and associated with small clusters of iron pyrite grains, are found in this facies. Dasyclad algae (*Tersella alpina*), rare ostracods and gastropods have also been observed (Fig. 3E).

The presence of oncoids and micritization processes points to an important algal and bacterial activity, which is compatible with low-energy, restricted shallow subtidal environments (Wilson 1975; Scholle et al. 1983). Beds are also rich in organic matter and pyrite. Thus, a low-energy, restricted (even anoxic) environment is assumed (Thévenard 1994).

Sand shoal facies association

This facies assemblage consists of fine to coarse-grained oolitic grain- to packstones (Fig. 3F) with subordinate shale and wackestone with ostracods, pelecypods and dasycladacea. Grainstone beds are typically 1–3 m thick and present two types of composition. The first type shows planar cross-bedded laminations, dipping 10 to 15° and is composed of well-sorted ooids, typically 0.3 to 0.5 mm in diameter, associated with various bioclasts (gastropods, pelecypods). All grains show early diagenetic cement which form clear spar isopachous rims around grains and in some cases a second generation of cement, consisting of asymmetrical cement. The second grainstone type is composed of well-sorted peloids (less than 0.1 mm in diameter) typically associated with benthic foraminifera (*Meandrospira sp.*, *Frondicularia* and *Glomospirella sp.*) and rare unidentified bryozoans. This subfacies frequently shows hummocky cross stratification and wave ripples. Isopachous rim cements are present but asymmetrical cements have never been observed. The shale facies is composed of black to dark grey, calcareous shale and forms decimetre-scale units passing upward into thick (50 cm to 1.5 m) bioclastic wackestone beds, rarely showing wave ripples. This wackestone is composed of a bioturbated micrite, containing rare intraclasts, ooids, lignite and various bioclasts: brachiopods, echinoid spines, rare foraminifera (miliolids). This facies is also characterized by decimetre-scale, nodular and elongate siliceous nodules.

The planar cross-bedded grainstones are interpreted as medium two dimensional subaqueous dunes with bedding produced by the migration of the bedform in a shallow subtidal environment (Ashley 1990). The peloid-miliolid grainstones are interpreted as subtidal facies (above the fare-weather wave base) subjected to sustained high-energy conditions (explaining sediments winnowing). The presence of HCS lamination and wave ripples rather than cross-bedded lamination tends to indicate wave and storm influence rather than a persistent current action. Benthic foraminifera and bryozoans point to an open shelf environment (Scholle et al. 1983; Tucker & Wright 1992), which is coherent with the previous assumption. The intercalation of grainstones with shales and wackestones suggests spatial and temporal variations in the energetic regime. Ooids point to a relative proximity to the subtidal dunes but the presence of brachiopod bioclasts, echinoid spines or rare miliolids are also indicative of open shelf conditions. These features suggest that fined-grained facies were deposited immediately backward of the subtidal dunes, in locally low-energy, shallow areas protected by these dunes.

Outer-shelf facies association

The subtidal shelf facies association includes three rock types: (1) shale; (2) crinoid and annelid wackestone; (3) sponge spicule wackestone. The shale facies is similar to the one of the previous association and consists of azoic, black to dark grey calcareous shale. The crinoid and annelid wackestone facies is present as 50 cm to 1 m thick, grey to brown layers, extending laterally for a few tens of metres to 100 m. This facies is composed of a dark micrite with crinoid bioclasts (Fig. 3G) and annelid tubes, associated with rare brachiopod bioclasts. Some rare sponge spicules have also been observed. The last facies of this association consists of a dark micrite with sponge spicules (Fig. 3H). Some rare centimetre-scale, nodular siliceous nodules are also present.

Crinoidal facies commonly develop in subtidal shelf environments, with the exception of sporadic occurrences in the platform interior (Della Porta et al. 2002). Actually, crinoids and annelids require open-marine, moderately agitated conditions below the effective wave base (Wilson 1975). This is confirmed by the wackestone texture, indicative of low-energy conditions and by brachiopod bioclasts also associated with open-marine environments. The presence of sponge spicules is characteristic of deeper water from lower ramp or outer subtidal settings (Wilson 1975).

High-frequency cyclicity of metre-scale cycles

Types of metre-scale cycles

In the platform carbonate successions, high-frequency metre-scale cycles (averaging 2–3 m) can be identified by the vertical facies arrangement. Two kinds of cycle are recognized (Fig. 2): peritidal cycles, capped by peritidal facies, and subtidal cycles, capped by shallow subtidal facies. Peritidal cycles are composed of peritidal facies and/or lagoonal facies. They show a shallowing-upward trend generally beginning with bioturbated/massive dolomite, passing upward into cryptalgal laminites and ending with facies characterized by exposure criteria:

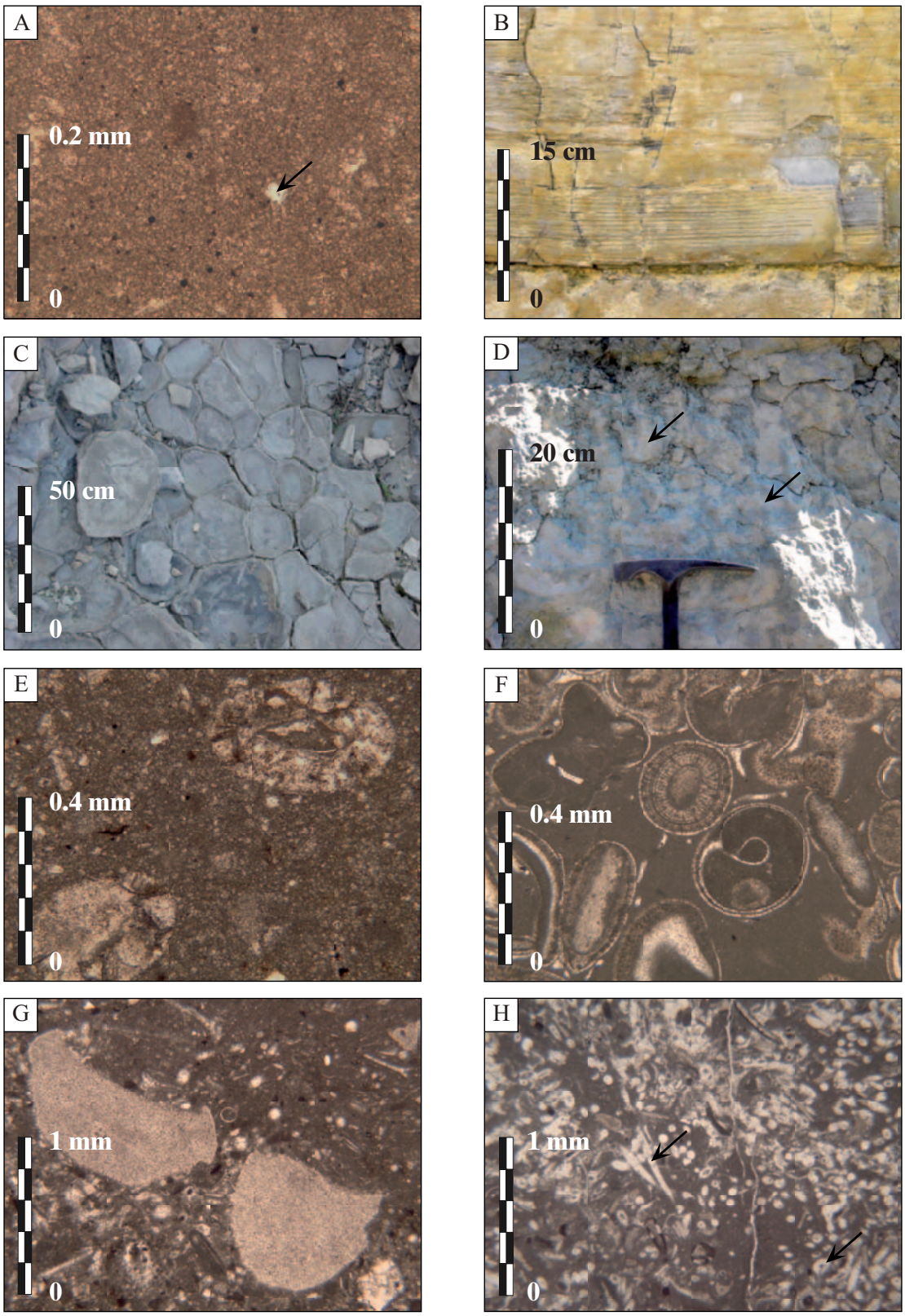

Fig. 3. **A.** Homogeneous dolomudstone. Rare quartz grains can be observed (Black arrow). **B.** Cryptalgal laminites (field photography). **C.** Plan view of polygonal desiccation cracks. **D.** Pedogenic horizon with decimetre-scale calcareous nodules (Black arrows). **E.** Wackestone with the dasyclad alga *Tersella alpina*. **F.** Oolitic and bioclastic packstone. **G.** Crinoid bioclasts of the crinoid and annelid wackestone facies. **H.** Sponge spicules wackestone facies (Black arrows).

Tab. 1. $\delta^{13}C$ and $\delta^{18}O$ values for Perthus samples. Sample labels refer to locations on the log in Fig. 5. Letters correspond to peritidal mudstone (PM); lagoonal wackestone (LW); lagoonal argillaceous mudstone (LAM); oolitic and bioclastic packstone (OBP); outer-shelf wackestone (OSW); black shales (BS).

Sample	Facies	$\delta^{13}C$ PDB	$\delta^{18}O$ PDB
P00	PM	0,52	-2,48
P01B	PM	-0,53	-5,01
P01	PM	-0,79	-5,25
P02	PM	0,55	-4,85
P03	PM	0,64	-3,76
P04	LW	0,12	-5,66
P05	LW	0,42	-4,28
P06	LW	0,63	-4,36
P07	PM	1,50	0,59
P08	PM	0,94	-1,94
P09	PM	1,13	-1,36
P10	PM	0,65	-3,80
P11	PM	0,75	-1,92
P12	PM	0,39	-0,79
P12B	LW	-0,13	-4,75
P13	LW	-0,52	-5,38
P13B	OBP	-0,02	-6,37
P14	OBP	0,95	-4,78
P15	LAM	1,16	-4,25
P16	OBP	-0,03	-4,59
P17	OBP	-0,05	-4,36
P18	OBP	0,31	-4,18
P19	PM	-0,16	-4,34
P20	OBP	1,35	-4,00
P21	OBP	1,26	-4,50
P22	OSW	1,61	-3,08
P23	OSW	1,86	-3,26
P24	OSW	2,10	-2,89
P25	OSW	1,74	-3,57
P26	OBP	1,04	-3,58
P27	OBP	0,89	-2,35
P28	OBP	1,02	-2,87
P29	BS	0,24	-3,78
P30	BS	0,03	-4,05
P31	BS	-0,21	-6,16
P32	BS	0,68	-3,61
P33	BS	-0,25	-3,67
P34	BS	0,38	-3,59
P35	BS	-0,10	-3,32

dessication polygons, pedogenic horizons or fenestral dolomite. Lagoonal facies also form laterally discontinuous cycles of 3 to 5 m thick, generally capped by peritidal facies (subaerial exposure facies), and thus can so be considered as peritidal cyles. Subtidal cycles are composed of sand shoal facies or outer-shelf facies. These cycles are basically shallowing-upward cycles without obvious evidence of prolonged subaerial exposure. Sand shoal facies form cycles of 3 to 5 m thick, presenting a shallowing-upward trend. These cycles generally begin with shale and cherty wackestone facies, passing upward into planar cross-bedded grainstone lithofacies. Outer-shelf facies form cycles several metres thick, displaying upward-increasing bed thickness. These cycles present a shale-rich lower part and a carbonate-rich upper part.

Certain peritidal and subtidal cycles show at their base a cross-laminated grainstone/packstone, passing upward into the previously mentioned evolution. The ravinement surface at the base of these cycles is associated to a transgressive surface and the grainstone/packstone facies represents a transgressive facies. These are usually too thin to show a deepening-upward facies succession, but the fact that they record coastal deposition after subaerial exposure indicates a relative sea-level rise. The upper-part of the cycle then shows a shallowing-upward facies.

Metre-scale cycles stacking pattern

Metre-scale cycles are commonly the basic building units of thick shallow-water carbonate successions and are commonly organized into relatively large-scale depositional sequences. Shallow-water carbonate successions are then characterized by a hierarchy of stratigraphic cyclicity (e.g. Osleger 1991; Strasser & Hillgärtner 1998). In the studied series, metre-scale cycles are organized in two large-scale cycles, generally ranging in thickness from 5 to 20 m, ranging from the uppermost part of unit 2 to lowermost part of unit 5 (Fig. 2). These large-scale cycles are deepening-shallowing cycles, usually capped by exposure surfaces commonly associated with paleosols or typical supratidal features. Correlations with other studies (Michard & Coumoul 1978; Perrisol 1990) enabled us to identify these two large-scale cycles as third-order depositional sequences (in the sense of Vail et al. 1977) and their component system tracts. The sequence boundary He3 and Si5 have thus been identified.

Isotopic data

Method

All samples were examined under cathodoluminescence (CL). The CL was performed using a Technosyn 8200 MkIV operating between 8 to 27 kV and 20 to 80 mA. Photographs were made on Spot RT camera associated with an Olympus BX40 microscope.

Sampling of carbonate powders was performed on fresh rock samples with a microdrill to avoid mixed components and late diagenetic veins and limited to the muddy part of each sample (micritic matrix for wackestone and packstone). Powders were roasted under vacuum at 380°C and were reacted with 100% phosphoric acid at 75° in an automated acid bath (online carbonate preparation line KARBO-KIEL). The resulting CO_2 was then analysed with a DELTA ADVANTAGE (Finnigan) mass spectrometer. The oxygen isotope ratios of the dolomitic facies (peritidal facies) were corrected for the different acid fractionation. Results are reported as $\delta^{13}C$ and $\delta^{18}O$ values relative to the PDB standard (Tab. 1). The analytical precision (standard deviation) based on duplicate analyses of each sample and on multiple analyses of carbonate standards was ± 0.03 ‰ for carbon and ± 0.05 ‰ for oxygen.

Results

Figures 4 and 5 show the results from the isotope analysis. Most data points fall within those documented for marine limestones (Moore 1989; Jenkyns & Clayton 1997; Jenkyns et al. 2002; Price & Gröcke 2002) and only a few points show an early meteoric diagenesis influence.

Measured $\delta^{13}C$ values range between -0.8‰ and +2.1‰. Outer-shelf facies reveal the most enriched $\delta^{13}C$ values, ranging from +1.6‰ to +2.1‰ (average +1.83‰; Fig. 4). In contrast to these micrites, carbonate muds deposited in the lagoonal and peritidal environments are depleted in ^{13}C: the lagoonal and peritidal micrites respectively reveal an average $\delta^{13}C$ value of +0.6‰ and +0.8‰. Oolitic and bioclastic packstones show similar values ranging from -0.02‰ to +1.4‰ (average +0.7‰). Finally, subaerial exposure facies present the most depleted values in $\delta^{13}C$ with an average $\delta^{13}C$ value of -0.3‰. The range of $\delta^{18}O$ values spans from -6.4‰ to +0.7‰ (Fig. 4). Subaerial exposure facies show the most depleted facies (average -4.8‰) and outer-shelf facies reveal more enriched $\delta^{18}O$ values, ranging from -3.6‰ to -2.9‰ (average -3.2‰; Fig. 4). Black shales show relatively depleted values (ranging from -0.3‰ to +0.7‰ for $\delta^{13}C$ and -6.2‰ to -3.3‰ for $\delta^{18}O$).

The isotopic trends plotted relative to stratigraphic position (Fig. 5, legend of Fig. 2) show marked variations: the $\delta^{13}C$ values show a minimum at the base of the section (label A) and then increase from -0.8‰ to 1.5‰ (label B). They decrease again to a distinct peak of -0.52‰ at 17m (label C; base of the *Turneri* zone), before presenting another increase to +2.11‰ at 37m (label D). After a new negative shift at 43m (label E), $\delta^{13}C$ curve increases to a mean value of 0–0.25‰ in the Toarcian unit. When plotted relative to stratigraphic position (Fig. 5), the variation of $\delta^{18}O$ is less obvious than that of $\delta^{13}C$. However, a similar evolution can be observed with a positive trend at 9m (label B), a negative one at 17m (label C) and a slightly increasing trend from 17m to 37m (label D). Comparison can be made between the sequence stratigraphic framework and isotopic curves (Fig. 5): 1) boundaries of the cycles are represented by depleted isotopic compositions; 2) maximum flooding surfaces are marked by enriched isotopic compositions; 3) the top discontinuity limiting the fourth lithological unit and corresponding to a major break in sedimentation does not show any specific isotopic signature, despite a closer sampling in the vicinity of the discontinuity.

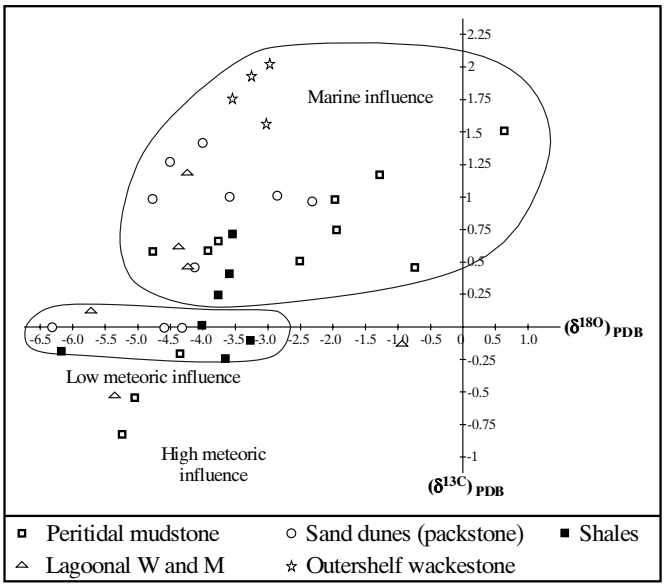

Fig. 4. Cross-plot of $\delta^{13}C$ vs. $\delta^{18}O$ values according to the facies of the analysed samples.

Evaluation of the data

Even if we selectively drilled the most homogeneous part of each sample for analysis, data must be evaluated for possible post-depositional alteration. Three points are evaluated and discussed here: effects of facies textures, secondary dolomitization and burial-related diagenetic alteration.

As previously mentioned, the sediments of the Perthus section were deposited under shallow-marine conditions. In this palaeogeographic context, lateral shifts of the depositional environments within the shelf can occur, resulting in vertical and lateral facies changes. In order to assess the impact of texture diversity on isotopic values (Vincent et al. 2004), a bivariate scatter of isotopic data has been associated with the texture of each sample (Fig. 4). Even if the textures of our samples range from mudstone to packstone, the isotopic data are not influenced by these variations: figure 4 does not show specific arrangement, neither for $\delta^{13}C$ nor for $\delta^{18}O$, which confirm that the variety of texture observed here do not influence $\delta^{13}C$ and $\delta^{18}O$ values. Moreover, potential intra-sample variations influences on the isotopic signals have been investigated. Several areas were microsampled from polished sections in six of our samples (Tab. 2). Each sample corresponds to a specific facies, in order to assess the impact of texture and lithology on intra-sample deviation. These analyses reveal a maximum range of intra-sample deviation for $\delta^{18}O$ of 0.52‰ and for $\delta^{13}C$ of 0.42‰. These two values correspond to the black shales sample, which also present "abnormal" depleted values (see above). This facies, corresponding to an open-marine facies should present normal marine values. The deviation and the low isotopic values observed for the black shale facies could be explained by a more heterogeneous composition than the micritic matrix of wackestones and packstones. Black shales also present a greater porosity and permeability than the limestone facies, which may induce potential interaction with current meteoric waters and explain these specific isotopic values. The other intra-sample variances do not exceed 0.35‰ for $\delta^{18}O$ and 0.33‰ for $\delta^{13}C$, which do not support very large intra-sample variations among our data. This seems to exclude samples heterogeneities and sampling artefacts.

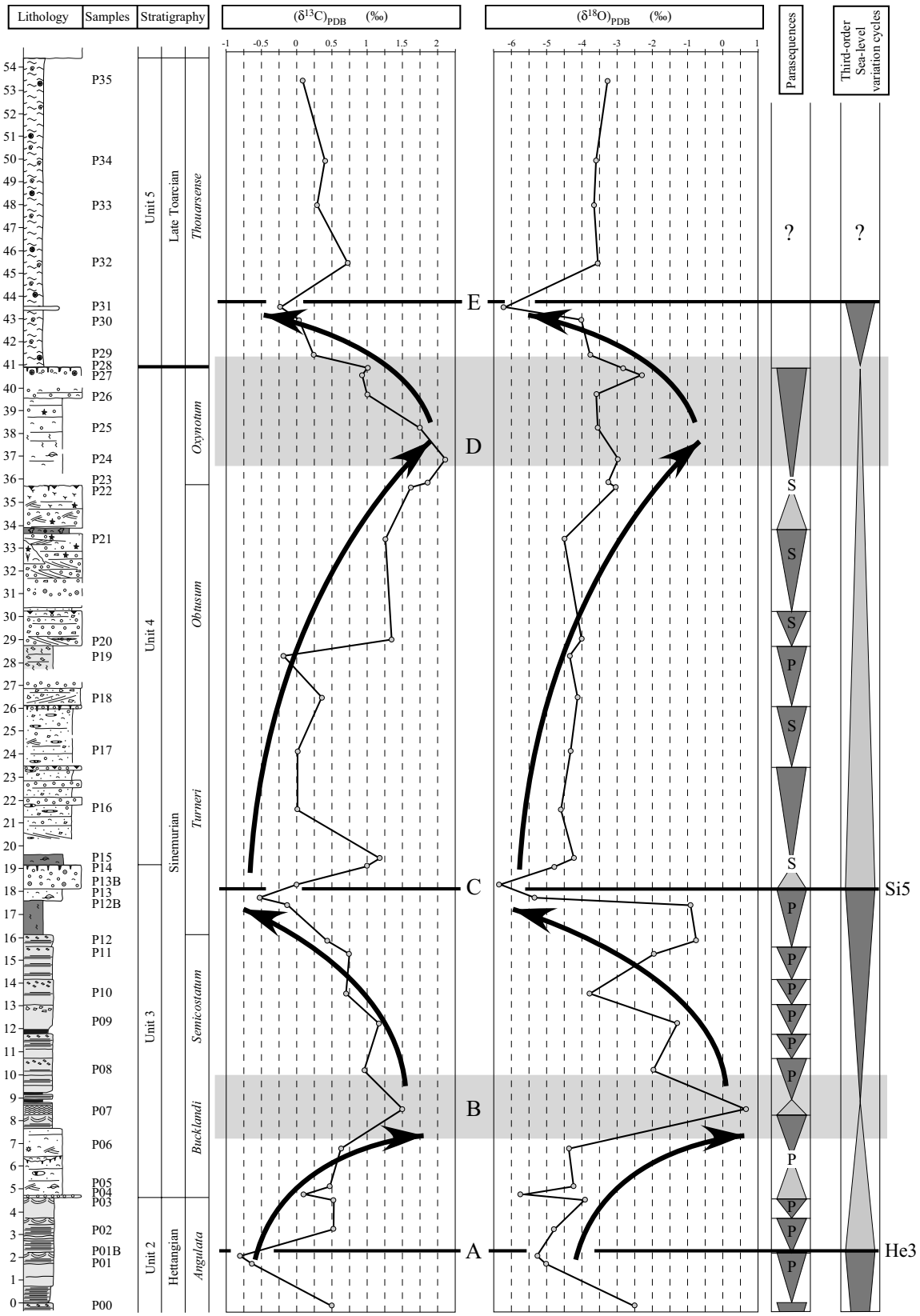

Fig. 5. Detailed Perthus section, with isotopic data and integrated biostratigraphy. Sequential framework is represented on the right (see text for explanation). Key on the log as in Fig. 2.

Tab. 2. Intra sample variability in $\delta^{13}C$ and $\delta^{18}O$ from representative facies of the Perthus samples. Letters as defined in table 1.

Facies	PM	LW	LAM	OBP	OSW	BS
Number of intra-sample measures	4	4	4	3	4	3
$\delta^{13}C$						
mean value (‰PDB	0.57	0.45	1.16	0.34	1.75	-0.27
range of varability (‰PDB)	0.18	0.33	0.32	0.25	0.24	0.42
standard deviation	0.03	0.02	0.04	0.02	0.02	0.05
$\delta^{18}O$						
mean value (‰PDB)	-4.77	-4.23	-4.22	-4.13	-3.57	-4.22
range of varability (‰PDB)	0.23	0.25	0.35	0.31	0.20	0.52
standard deviation	0.06	0.06	0.04	0.03	0.04	0.06

In order to evaluate the effects and extent of secondary dolomitization, thin sections of all samples have been examined under plane light for preservation of microfabrics and presence of diagenetic features. Characteristic facies (Fig. 3) are compared to two samples affected by secondary dolomitization (Fig. 6). The first stage of secondary dolomitization consists of subhedral to anhedral dolomite crystals ranging in size from 50 to 100 µm. These crystals are preferentially observed in partial replacement of precursor grains (ooids, bioclasts), rarely in the micritic matrix of the facies (Fig. 6A). The last stage of secondary dolomitization consists of crystalline dolomite, brown or grey in hand specimen. Precursor fossils or fine-scale sedimentary textures are completely obliterated. This fabric is composed of anhedral to subhedral dolomite crystals, ranging from 100 to 300 µm that replace precursor grains and cements (Fig. 6B). Some crystals have a cloudy centre and a clear rim. The samples on which we performed isotopic measures do not show any trace of secondary dolomitization and we can exclude alteration of the primary C and O isotopic compositions by this phenomenon.

All samples were then examined under cathodoluminescence (CL), in order to have information on the environment of precipitation, burial history and timing of diagenesis. CL depends on the Eh-conditions in the diagenetic environment and on the abundance of specific trace and REE elements. The different cements and matrix have therefore been examined: Micritic matrix of our samples shows dull to very dull orange CL-colour (Figs. 7A and 7B). Any luminescence of micrites is indicative of diagenetic recrystallisation. However, this does not necessarily mean that the carbon isotope signals will be erased. As long as diagenetic stabilisation and cementation proceeds in a system closed for carbon, the $\delta^{13}C$ signals of the precursor will be inherited by the recrystallized carbonate. Clear spar isopachous rims ranging from 10 to 15 µm in thickness (Figs. 7C and 7D), growing from the grain wall, present a non-luminescent fabric, typical of marine phreatic cement (Nelson & James 2000). For comparison, a pack/grainstone with burial cement between grains is presented (Figs. 7E and 7F). This cement shows a bright yellow-orange CL-colour.

The fact that each cement presents a luminescence reflecting its composition and origin tends to indicate a minor burial overprint. In order to confirm this hypothesis, three others points can be advanced. Firstly, the lack of trace of compaction (pressure-solution, grains fragmentation) tends to indicate a relatively low burial. Moreover, mineralogical analysis (X-Ray diffraction) lead on clay fraction of the lagoonal facies (Mélas 1982) have shown that clay minerals are mainly composed of illite and kaolinite (in lower proportion). On X-Ray diagrams, illites present a high width at mid-height of the 10Å illite peak.

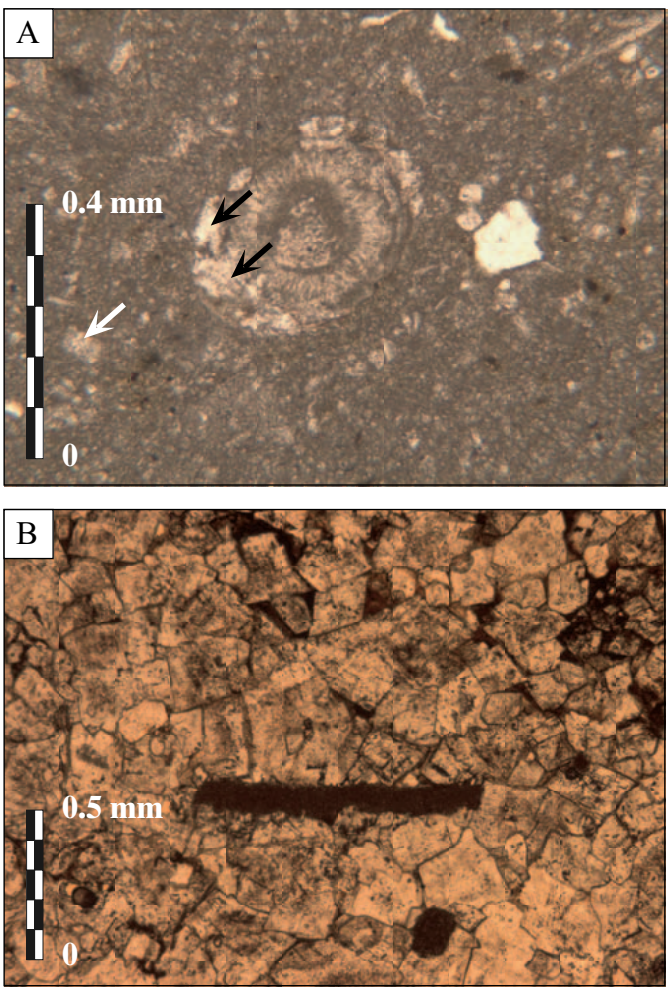

Fig. 6. **A.** First stage of dolomitization observed in a lagoonal wackestone. Crystals of dolomite have begun to replace a precursor ooids (black arrows). Some subhedral crystals are also present in the micrite (White arrow). **B.** Crystalline dolomite composed of anhedral to subhedral dolomite crystals. Some crystals have a cloudy centre.

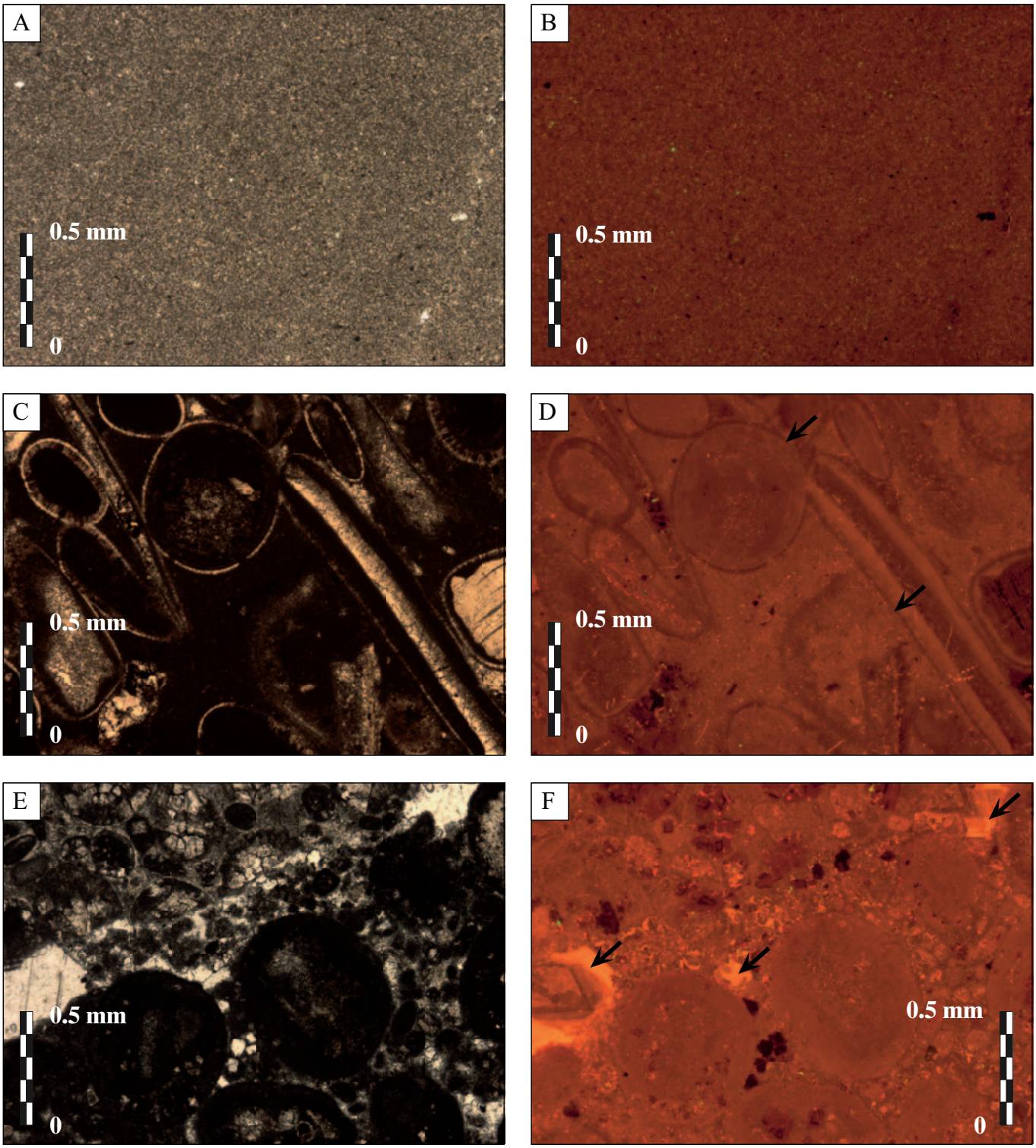

Fig. 7. **A. & B.** Homogeneous mudstone examined under plane light and under cathodoluminescence. This micritic facies shows a dull to very dull orange CL-colour. **C. & D.** Oolitic and bioclastic packstone examined under plane light and under cathodoluminescence. The micritic matrix of the facies shows a dull orange CL-colour. Black arrows point to non-luminescent clear spar isopachous rims around grains typical of marine phreatic cement. **E. & F.** For comparison, a pack/grainstone is examined under plane light and under cathodoluminescence. This facies shows burial cement in the porosity (black arrows), coloured in bright yellow-orange under cathodoluminescence.

This is typical of low cristallinity index that points to a detrital origin of illite. On the contrary, a high cristallinity index would have indicated diagenetic neoformation of illite (Biscaye 1965; Dunoyer De Segonzac 1969). This observation tends to confirm a relatively low burial diagenesis.

Secondly, diagenetic alteration of the $\delta^{13}C$ signal by burial diagenesis can be detected by a strong correlation between $\delta^{13}C$ and $\delta^{18}O$ values (correlation coefficient = 1; Brasier et al. 1996; Shen & Schidlowski 2000). The correlation coefficient for two sets of data has been defined as:

$$px.y = \frac{Cov(X, Y)}{ox \cdot oy}$$

where X and Y are the sample means of the two sets of data (here $\delta^{13}C$ and $\delta^{18}O$ values). The correlation coefficient calculated for our data is 0.43, which can be considered significantly inferior to 1. Absence of correlation between $\delta^{13}C$ and $\delta^{18}O$ seems therefore to exclude burial diagenetic alteration of the early C and O isotopic compositions.

Finally, the C and O isotope values have been associated with the facies type of each sample (Fig. 4). The data that represent the outer-shelf facies trend towards the higher, open-marine values and away from early meteoric and burial values. On the contrary, the data that represent the peritidal and lagoonal facies trend towards the early meteoric values. It is therefore argued that even if some burial resetting of the primary micrite $\delta^{13}C$ and $\delta^{18}O$ values have occurred, broad trends in marine environmental and early meteoric signatures are preserved.

Discussion: Origin of the isotopic signal

Three mechanisms are generally invoked for explaining isotopic variations in shallow-water platform carbonates: 1) $\delta^{13}C$ and $\delta^{18}O$ fluctuations in global sea-water geochemistry; 2) sea water ageing related to long residence time of water masses in shallow, poorly circulated settings; 3) early meteoric diagenesis during exposure periods (low values of the exposure facies are generally interpreted to be related to the influence of ^{18}O-depleted early meteoric fluids and ^{13}C-depleted soil-zone CO2; Allan & Matthews 1982).

Numerous authors have demonstrated that shallow-platform carbonates have the potential for providing an excellent record of sea level, especially during periods of high-amplitude oscillations. During the late Pleistocene, shallow-platform carbonates can be correlated with the deep-sea isotope proxy of sea-level change (Vahrenkamp 1996; Kievman 1998). Jenkyns et al. (2002) have published a carbon isotope curve for the Jurassic, derived from a compilation of marine (belemnite) isotope data and that is suggested to show global trends. They have shown "a possible negative excursion in Hettangian time followed by a positive excursion centred in mid-Sinemurian time and subsequently by a well-defined negative excursion around the Sinemurian-Pliensbachian boundary". Hettangian time is out of the scope of this article, but a positive interval is observed here, at 37m, in the *Turneri* zone (mid-Sinemurian time). It is however difficult to correlate these positive excursions because of the lack of precise biostratigraphic framework for the Jurassic curve of Jenkyns et al. (2002). Actually, the lack of published high-resolution isotope profiles for Sinemurian times precluded us from comparing and correlating our data with other locations or sedimentary environments. An important number of publications has documented the carbon and oxygen isotope evolution in the upper part of the Liassic series, from Pliensbachian to Toarcian times (Jenkyns & Clayton 1997; Hesselbo et al. 2000; Rosales et al. 2001; Morettini et al. 2002; Rey & Delgado 2002; Bailey et al. 2003; Rosales et al. 2004a; Rosales et al. 2004b). However, only a few studies have been published on isotopic evolution of Hettangian-Sinemurian series (Azzaro et al. 1993; Qing et al. 2001) and no high-resolution isotope profile tied with biostratigraphic data exist.

Moreover, our data are derived from shallow-water carbonates, which are likely to reflect local trends or early diagenesis. In this particular setting, sea water ageing may explain $\delta^{13}C$ fluctuations. In shallow water environments (waters that had limited exchange with the open ocean), the carbon isotope ratios may change due to remineralisation of organic carbon (^{13}C depletion) or enhanced photosynthesis (^{13}C enrichment), all of which occur as the water mass "ages" (Patterson & Walter 1994; Holmden et al. 1998; Immenhauser et al. 2002; Immenhauser et al. 2003). These authors thus linked the $\delta^{13}C$ depletion to the input of ^{12}C from remineralized organic carbon during the long residence time of seawater on the platform. It is however difficult to invoke ageing phenomenon in our case study. Firstly, only a few points (corresponding to distinct negative peaks in the figure 5) are ^{13}C-depleted, and the major part of our data presents normal sea-water values. It is therefore necessary to invoke episodic restriction related to low relative-sea level (depleted isotopic compositions correspond to third-order sequence boundary), but no sedimentary features support the hypothesis of periods of water-mass restriction. ^{13}C-depleted values are obtained from different facies such as peritidal mudstone, lagoonal wackestone and oolitic/bioclastic packstone (2D dunes). Secondly, although sea-water ageing can result in depleted ^{13}C due to remineralization of organic carbon, it would likely result in enriched ^{18}O explained by respiration and photosyntesis (Magaritz & Stemmerik 1989; Patterson & Walter 1994). Figure 5 shows that ^{13}C-depleted values are correlated with ^{18}O-depleted values, which tend to eliminate sea-water ageing as controlling factor.

Early diagenetic alteration may readily explain the depleted composition in $\delta^{13}C$ and $\delta^{18}O$. The low $\delta^{13}C$ values could be related to the influence ^{13}C-depleted soil-zone CO_2 that affected the bulk isotopic composition of supratidal facies (Allan & Matthews 1977; Allan & Matthews 1982; Immenhauser et al. 2003). Indeed, negative carbon isotope trends are commonly believed to result from the uptake of light carbon derived from the deterioration of organic material in soils during subaerial exposure (Allan & Matthews 1982; Lohman 1988; Sattler et al. 2005). The depleted composition of $\delta^{18}O$ could be explained

by the influence of ^{18}O-depleted early meteoric fluids linked to meteoric diagenesis of marine carbonates above the water table. This hypothesis is support by the fact that third-order cycle boundaries are marked by supratidal facies (desiccation cracks, fenestrae, pedogenic horizons) and traces of early vadose diagenesis (drusy calcite along the fenestrae walls).

However, other emersion surfaces have been observed in the series, corresponding to boundaries of high-order cycles (metre-scale cycles, Fig. 5). These boundaries do not present significantly depleted signatures, even if in the field they can show the same characteristics that third-order cycle boundaries. The relationship between the duration of subaerial exposure and the resulting diagenetic alteration of the isotope ratios was investigated by Joachimski (1994). Potentially, metre-scale cycles boundary do not represent the same duration of exposure, amplitude of relative sea-level fall and lateral extension of the exposed surfaces than third-order cycles. Indeed, long subaerial exposure represented by third-order cycle boundaries would promote greater equilibration with isotopically light, soil-derived CO_2 and ^{18}O-depleted early meteoric fluids. Moreover, third-order sequence boundaries can be correlated over the whole platform across distances up to tens of kilometres, whereas metre-scale cycles boundaries have a limited lateral extension (Hamon et al. 2005). These two factors may explain the different responses of third-order and metre-scale cycles boundaries.

On the contrary, enriched isotopic compositions are observed on the Perthus section at 8 m and 37 m (label B and D, Fig. 5) and are correlated with the maximum flooding surfaces of the third-order cycles. These high isotopic values point to a limited effect or even a lack of meteoric diagenesis, indicative of marine conditions. Isotopic characterization for maximum flooding surfaces is less precise than for sequence boundaries, indicating a strong but localized effect of the meteoric influence. Finally, the absence of specific signature of the top hardground could be explained by its complexity. Actually, previous authors (Aubague & Lefavrais-Raymond 1974; Lefavrais-Raymond & Lablanche 1985; Mattei 1985) have shown that this discontinuity recorded several episodes of sedimentary condensation, subaerial exposure and erosion. The latter might have removed part of the sedimentary succession, thus erasing the primary signature of this surface (boundary of third-order cycle).

Conclusions

This study reports geochemical data from the early Liassic succession of the Lodève region. This work is based on the oxygen and carbon stable isotopic stratigraphy of a shallow marine carbonate platform that we interpret as related to third-order sea-level variations cycles rather than to global environmental changes.

Boundaries of third-order cycles are represented by depleted isotopic compositions and maximum flooding surfaces are marked by enriched isotopic compositions. However, high-order cycles boundaries, such as parasequence boundaries, do not present specific signatures. This point can be considered as a good tool to distinguish third-order sequence boundaries among other emersion surfaces, observed in diagenetic unaltered shallow carbonate series.

Acknowledgements

We wish to thank reviewers R. Martini, M. Joachimsky and an anonymous reviewer and editor D. Ariztegui for their helpful comments that greatly improved the original manuscript.

REFERENCES

Ali, M. Y. 1995: Carbonate cement stratigraphy and timing of diagenesis in a Miocene mixed carbonate-clastic sequence, offshore Sabah, Malaysia: constraints from cathodoluminescence, geochemistry, and isotope studies. Sedimentary Geology 99, 191–214.

Allan, J. R. & Matthews, R. K. 1977: Carbon and oxygen isotopes as diagenetic and stratigraphic tools: Surface and subsurface data, Barbados, West Indies. Geology 5, 16–20.

Allan, J. R. & Matthews, R. K. 1982: Isotope signatures associated with early meteoric diagenesis. Sedimentology 29, 797–817.

Ashley, G. M. 1990: Classification of large-scale subaqueous bedforms: new look at an old problem. Journal of Sedimentary Petrology 60, 160–172.

Aubague, M. & Lefavrais-Raymond, A. 1974: Lias et Dogger de la bordure cévenole (Retombée orientale du dôme de Gorniès). Implications paléogéographiques. Bulletin du BRGM 2, 49–64.

Azzaro, E., Bellanca, A. & Neri, R. 1993: Mineralogy and geochemistry of Mesozoic black shales and interbedded carbonates, southeastern Sicily: evaluation of diagenetic processes. Geological Magazine 130, 191–202.

Bailey, T. R., Rosenthal, Y., McArthur, J. M., Van De Schootbrugge, B. & Thirlwall, M. F. 2003: Paleoceanographic changes of the Late Pliensbachian-Early Toarcian interval: a possible link to the genesis of an Oceanic Anoxic Event. Earth and Planetary Science Letters 212, 307–320.

Baudrimont, A. F. & Dubois, P. 1977: Un Bassin Mésogéen du domaine périalpin: Le Sud-Est de la France. Bulletin des Centres de Recherches et d'-exploration-Production Elf Aquitaine 1, 261–308.

Biscaye, P. E. 1965: Mineralogy and sedimentation of recent deep-sea clay in the Atlantic Ocean and adjacent seas and oceans. Geological Society of America Bulletin 76, 803–832.

Brasier, M. D., Shields, G., Kuleshov, V. N. & Zhegallo, E. A. 1996: Integrated chemo- and biostratigraphic calibration of early animal evolution: Neoproterozoic-Early Cambrian of southwest Mongolia. Geological Magazine 133, 445–485.

Buonocunto, F. P., Sprovieri, M., Bellanca, A., D'Argenio, B., Ferreri, V., Neri, R. & Ferruza, G. 2002: Cyclostratigraphy and high-frequency carbon isotope fluctuations in Upper Cretaceous shallow-water carbonates, southern Italy. Sedimentology 49, 1321–1337.

Corbin, J.-C., Person, A., Iatzoura, A., Ferre, B. & Renard, M. 2000: Manganese in pelagice carbonates: indication of major tectonic events during the geodynamic evolution of a passive continental margin. (The Jurassic European Margin of the Tethys-Ligurian Sea). Palaeogeography, Palaeoclimatology, Palaeoecology 156, 123–138.

Craig, H. 1965: The measurement of oxygen isotope paleotemperatures. Earth and Planetary Science Letters 5, 837–858.

Debrand-Passard, S., Courbouleix, S. & Lienhardt, M.-J. 1984: Synthèse géologique du Sud-Est de la France. Stratigraphie et paléogéographique. BRGM, Orléans, 615 pp.

Della Porta, G., Kenter, J. A. M., Immenhauser, A. & Bahamonde, J. R. 2002: Lithofacies character and architecture across a Pennsylvanian inner-platform transect (Sierra de Cuera, Asturias, Spain). Journal of Sedimentary Research 72, 898–916.

Dunoyer De Segonzac, G. 1969: Les mineraux argileux dans la diagenese. Passage au metamorphisme. Thèse de doctorat, Faculté des Sciences de Strasbourg, Strasbourg, 320 pp.

Hamon, Y., Merzeraud, G. & Combes, P.-J. 2005: Des cycles haute fréquence de variations du niveau marin relatif enregistrés dans les discontinuités sédimentaires: un exemple dans le Lias inférieur de Lodève (Sud-Est de la France). Bulletin de la Société Géologique de France 176, 57–68.

Hesselbo, S. P., Meister, C. & Gröcke, D. R. 2000: A potential global stratotype for the Sinemurian-Pliensbachian boundary (Lower Jurassic), Robin Hood's Bay, UK: ammonite faunas and isotope stratigraphy. Geological Magazine 137, 601–607.

Holmden, C., Creaser, R. A., Muehlenbachs, K., Leslie, S. A. & Bergström, S. M. 1998: Isotopic evidence forgeochemical decoupling between ancient epeiric seas and bordering oceans: Implications for secular curves. Geology 26, 567–570.

Immenhauser, A., Della Porta, G., Kenter, J. A. M. & Bahamonde, J. R. 2003: An alternative model for positive shifts in shallow-marine carbonate $\delta^{13}C$ and $\delta^{18}O$. Sedimentology 50, 953–959.

Immenhauser, A., Kenter, J. A. M., Ganssen, G., Bahamonde, J. R., Van Vliet, A. & Saher, M. H. 2002: Origin and significance of isotope shifts in Pennsylvanian carbonates (Asturias, NW Spain). Journal of Sedimentary Research 72, 82–94.

Ingram, B. L., Conrad, M. E. & Ingle, J. C. 1996: Stable isotope and salinity systematic in estuarine waters and carbonates: San Francisco Bay. Geochimica Cosmochimica Acta 60, 455–468.

Jenkyns, H. C. & Clayton, C. J. 1997: Lower Jurassic epicontinental carbonates and mudstones from England and Wales: chemostratigraphic signals and the early Toarcian anoxic event. Sedimentology 44, 687–706.

Jenkyns, H. C., Jones, C. E., Gröcke, D. R., Hesselbo, S. P. & Parkinson, D. N. 2002: Chemostratigraphy of the Jurassic System: applications, limitations and implications fot palaeoceanography. Journal of the Geological Society of London 159, 351–378.

Joachimski, M. M. 1994: Subaerial exposure and deposition of shallowing upward sequences: evidence from stable isotopes of Purbeckian peritidal carbonates (basal Cretaceous), Swiss and French Jura Mountains. Sedimentology 41, 805–824.

Kievman, C. M. 1998: Match between late Pleistocene Great Bahama Bank and deep-sea oxygen isotope records of sea level. Geology 26, 635–638.

Lefavrais-Raymond, A. & Lablanche, G. 1985: Contrôle tectonique de la sédimentation du Lotharingien à l'Aalénien sur le Seuil Caussenard. Cahiers de l'institut catholique de Lyon 14, 191–201.

Lohman, K. C. 1988: Geochemical patterns of meteoric diagenetic systems and their application to studies of paleokarst. In: James, N. P. & Choquette, P. W. (Eds.): Paleokarst, Springer, Berlin, 58–80.

Lopez, M. 1992: Dynamique du passage d'un appareil terrigène à une plateforme carbonatée en domaine semi-aride: Le Trias de Lodève, Sud de la France. Thèse de Doctorat, Université Montpellier 2, Montpellier, 403 pp.

Machel, H. G., Mason, R. A., Mariano, A. N. & Mucci, A. 1991: Causes and emission of luminescence in calcite and dolomite. In: Barker, C. E. & Kopp, O. C. (Eds.): Luminescence microscopy: Quantitative and qualitative aspects. SEPM Short Course (25), Houston, Texas, 9–25.

Magaritz, M. & Stemmerik, L. 1989: Oscillation of carbon and oxygen isotopic compositions of carbonate rocks between evaporative and open marine environments, Upper Permian of East Greenland. Earth and Planetary Science Letters 93, 233–240.

Marza, P., Seguret, M. & Moussine-Pouchkine, A. 1998: Application du Fischer plot et de l'analyse spectrale a la cyclostratigraphie d'une serie peritidale discontinue; exemple du Lias carbonate, bordure sud du Causse du Larzac, France. Bulletin de la Société Géologique de France 169, 547–562.

Mattei, J. 1985: Application de méthodes d'analyse globale à l'étude des Amalthéidés du bassin sédimentaire des Causses du Sud du Massif Central Français (Carixien supérieur et Domérien). Editions du CNRS, Paris, 146 pp.

Mélas, P. 1982: Etude sédimentologique, paléogéographique et géochimique du Lias carbonaté du Nord-Lodévois. Application à la reconnaissance et à l'interprétation d'amas métallifères. Thèse de Doctorat, Université Montpellier 2, Montpellier, 419 pp.

Michard, A. G. & Coumoul, A. 1978: La sédimentation liasique dans les Causses: Contrôle des minéralisations Zn-Pb associées au Lotharingien. Bulletin du BRGM 2, 57–120.

Moore, C. H. 1989: Carbonate Diagenesis and Porosity. Elsevier, New York, 338 pp.

Morettini, E., Santantonio, M., Bartolini, A., Cecca, F., Baumgartner, P. O. & Hunziker, J. C. 2002: Carbon isotope stratigraphy and carbonate production during the Early-Middle Jurassic: examples from the Umbria-Marche-Sabina Apennines (central Italy). Palaeogeography, Palaeoclimatology, Palaeoecology 184, 251–273.

Nelson, C. S. & James, N. P. 2000: Marine cements in mid-Tertiary cool-water shelf limestones of New Zealand and Southern Australia. Sedimentology 47, 609–629.

Osleger, D. 1991: Subtidal carbonate cycles: Implications for allocyclic vs. autocyclic controls. Geology 19, 917–920.

Patterson, W. P. & Walter, L. M. 1994: Depletion of ^{13}C in seawater ΣCO_2 on modern carbonate platforms: Significance for the carbon isotopic record of carbonates. Geology 22, 885–888.

Perrisol, M. 1990: Sédimentologie et metallogénie du Trias et du Lias carbonaté de la bordure Cévenole. Thèse de Doctorat, Université Montpellier 2, Montpellier. 575 pp.

Pratt, B. R., James, N. P. & Cowan, C. A. 1992: Peritidal carbonates. In: Walker, R. G. & James, N. P. (Eds.): Facies models: Response to sea level change. Geological Association of Canada, 303–322.

Price, G. D. and Gröcke, D. R. 2002: Strontium-isotope stratigraphy and oxygen- and carbon-isotope variation during the Middle Jurassic-Early Cretaceous of the Falkland Plateau, South Atlantic. Palaeogeography, Palaeoclimatology, Palaeoecology 183, 209–222.

Qing, H., Bosence, D. W. J. & Rose, E. P. F. 2001: Dolomitization by penesaline sea water in Early Jurassic peritidal platform carbonates, Gibraltar, western Mediterranean. Sedimentology 48, 153–163.

Renard, M. 1984: Géochimie des carbonates pélagiques: mise en évidence de la fluctuation de la composition des eaux océaniques depuis 140 Ma, essai de chimiostratigraphie. Doc. BRGM 85, 1–650.

Rey, J. & Delgado, A. 2002: Carbon and oxygen isotopes: a tool for Jurassic and early Cretaceous pelagic correlation (southern Spain). Geological Journal 37, 337–345.

Rosales, I., Quesada, S. & Robles, S. 2001: Primary and diagenetic isotopic signals in fossils and hemipelagic carbonates: the Lower Jurassic of northern Spain. Sedimentology 48, 1149–1169.

Rosales, I., Quesada, S. & Robles, S. 2004a: Paleotemperature variations of Early Jurassic seawater recorded in geochemical trends of belemnites from the Basque-Cantabrian basin, northern Spain. Palaeogeography, Palaeoclimatology, Palaeoecology 203, 253–275.

Rosales, I., Robles, S. & Quesada, S. 2004b: Elemental and oxygen isotope composition of Early Jurassic belemnites: salinity vs. temperature signals. Journal of Sedimentary Research 74, 342–354.

Sattler, U., Immenhauser, A., Hillgärtner, H. & Esteban, M. 2005: Characterization, lateral variability and lateral extent of discontinuity surfaces on a carbonate platform (Barremian to lower Aptian, Oman). Sedimentology 52, 339–361.

Scholle, P. A., Bebout, D. G. & Moore, C. H. (Eds.) 1983: Carbonate depositional environments. AAPG memoir (33), Tulsa, Oklahoma. 780 pp.

Shen, Y. & Schidlowski, M. 2000: New C isotope stratigraphy from southwest China: Implications for the placement of the Precambrian-Cambrian boundary on the Yangtze Platform and global correlations. Geology 28, 623–626.

Strasser, A. & Hillgärtner, H. 1998: High-frequency sea-level fluctuations recored on a shallow carbonate platform (Berriasian and Lower Valanginian of Mount Salève, French Jura). Eclogae Geologicae Helvetiae 91, 375–390.

Thévenard, F. 1994: Plant beds: stratigraphical key beds or relative low sea-level indicators? Comptes-Rendus de l'Académie des Sciences de Paris 318, 137–143.

Tucker, M. E. & Wright, V. P. 1992: Carbonate Sedimentology. Blackwell Scientific Publications, Oxford. 482 pp.

Vahrenkamp, V. C. 1996: Carbon isotope stratigraphy of the Upper Kharaib and Shuaiba formations: Implications for the Early Cretaceous evolution of the Arabian Gulf region. AAPG bulletin 80, 647–662.

Vail, P. R., Mitchum, R., Todd, R. G., Widmier, J. M., Thompson, S., Sangree, J., Bubb, J. N. & Hatlelid, W. G. 1977: Seismic stratigraphy and global changes of sea level. In: Payton, C. E. (Ed.), AAPG Memoir (26), Tulsa, Oklahoma. 49–112.

Valladares, I., Recio, C. & Lendinez, A. 1996: Sequence stratigraphy and stable isotopes ($\delta^{13}C$, $\delta^{18}O$) of the Late Cretaceous carbonate ramp of the Western margin of the Iberian Chain (Soria Spain). Sedimentary Geology 105, 11–28.

Veizer, J., Ala, D., Azmy, K., Bruckschen, P., Buhl, D., Bruhn, F., Cardem, G. A. F., Diener, A., Ebneth, S., Godderis, Y., Jasper, T., Korte, C., Pawellek, F., Podlaha, O. G. & Strauss, H. 1999: ^{87}Sr / ^{86}Sr, $\delta^{13}C$ and $\delta^{18}O$ evolution of Phanerozoic seawater. Chemical geology 161, 59–88.

Vincent, B., Emmanuel, L. & Loreau, J.-P. 2004: Signification du signal isotopique ($\delta^{18}O$, $\delta^{13}C$) des carbonates néritiques: composante diagénétique et comosante originelle (Jurassique supérieur de l'Est du bassin de Paris, France). Comptes-Rendus Géoscience (Géochimie) 336, 29–39.

Wilson, J. L. 1975: Carbonate facies in Geologic History. Springer-Verlag, Berlin Heidelberg New York, 471 pp.

Zeebe, R. E. 2001: Seawater pH and isotopic paleotemperatures of Cretaceous ocean. Palaeogeography, Palaeoclimatology, Palaeoecology 170, 49–57.

Manuscript received June 28, 2005
Revision accepted July 24, 2006
Published Online First April 18, 2007